Chinese Journal of Chemical Engineering 82 (2025) 67–82

Contents lists available at ScienceDirect

Chinese Journal of Chemical Engineering

journal homepage: www.elsevier.com/locate/CJChE

Full Length Article

Experimental research on the macro- and micro-mixing in the low-density polyethylene autoclave reactor

Zhenchao Tang [1], Yuliang Wang [1], Zhengliang Huang [1], Yao Yang [1,*], Xiaoqiang Fan [1,2,*], Binbo Jiang [1], Jingdai Wang [1], Yongrong Yang [1]

[1] State Key Laboratory of Chemical Engineering, College of Chemical and Biological Engineering, Zhejiang University, Hangzhou 310027, China
[2] Ningbo Innovation Center, Zhejiang University, Ningbo 315100, China

ARTICLE INFO

Article history:
Received 1 July 2024
Received in revised form
17 December 2024
Accepted 17 December 2024
Available online 19 March 2025

Keywords:
Low-density polyethylene (LDPE)
Autoclave reactor
Macro-mixing
Micro-mixing
Characteristic time

ABSTRACT

It has been widely recognized that the mixing process has significant impacts on the performance of low-density polyethylene (LDPE) reactors due to the rapid radical polymerization occurred in the reactors, but how the macro- and micro-mixing affect the reactor performance was still controversial in publications. In this work, a cold-flow LDPE autoclave with multi-feedings was scaled down (1/2) from an industrial reactor and built to systematically investigate the macro- and micro-mixing characteristics of fluid by experiments. Furthermore, the effects of macro- and micro-mixing on the polymerization were comprehensively analyzed. The results showed that according to the delay time t_d and macro-mixing times t_M calculated from residence time distribution (RTD) curves, the macro-mixing states are significantly different at various axial positions (h/H), especially at lower agitation Reynolds number *Re*. But with the increase of *Re*, since the circulation flow in the reactor is strengthened, the t_d for each feed gradually decreases to 0, and the t_M at different axial positions tend to be identical. For micro-mixing, the qualities of micro-mixing at different axial positions are similar, and the average micro-mixing time $\overline{t_m}$ in the reactor decreases exponentially with the increase of *Re*. Moreover, a fitting model was established. Through the comparison of the characteristic times of macro-mixing (t_d, t_M), micro-mixing ($\overline{t_m}$) and elementary reactions within the industrial range of *Re*, it can be concluded that the properties of LDPE products are dominated by the macro-mixing behavior, and the consumption of initiators is affected by both the macro- and micro-mixing behaviors. This conclusion is of great significance for the design, optimization and operation of LDPE reactors.

1. Introduction

Low-density polyethylene (LDPE) is a thermoplastic resin, widely used in film, molding materials, coating materials, plate materials, electrical insulating materials, *etc*. [1]. The reactors to produce LDPE are commonly operated at high temperature (150–280 °C) and high pressure (130–250 MPa) *via* a series of fast free-radical reactions, including the elementary reactions of initiator decomposition, chain initiation, chain propagation, chain transfer to monomer, chain transfer to polymer, chain transfer to solvent, chain termination by disproportionation and chain termination by combination [2–4].

It has been widely accepted in the related research field that the performance of LDPE reactors is significantly affected by the mixing characteristics of fluid [5–8], thus the LDPE products synthesized in autoclave reactors and tubular reactors have significant differences in molecular structures. In general, the LDPE produced in the autoclave reactor has more long chain branched structures and wider molecular weight distribution, due to the much more complex mixing behaviors in the LDPE autoclave reactor [9]. Therefore, the research on the mixing characteristics of fluid in LDPE autoclave reactors is of great importance in regulating the product properties.

The fluid mixing in autoclave reactors goes through the processes of macro-mixing and micro-mixing. The macro-mixing is the mixing process on the reactor scale through turbulent diffusion and convection, and the micro-mixing is the mixing process on the molecular scale through molecular diffusion and viscous deformation [10,11]. For studying the effects of the mixing characteristics

* Corresponding authors.
E-mail addresses: yao_yang@zju.edu.cn (Y. Yang), fanxq@zju.edu.cn (X. Fan).

https://doi.org/10.1016/j.cjche.2024.12.023

of fluid on the performance of LDPE autoclave reactors, the prerequisite is to determine which scale of mixing dominates the polymerization, but this issue is still unresolved in the literatures.

Numerous researchers have investigated effects of the macro-mixing characteristics of fluid on the performance of LDPE autoclave reactors. Marini and Georgakis [5] and Ochs *et al.* [6] used a three-zone model to characterize the non-ideal macro-mixing in an LDPE autoclave reactor, and predicted the dependence of initiator consumption on the operating temperature by the proposed reactor model. Zhang and Ray [7] researched the effects of imperfect macro-mixing on the properties of LDPE product by using a three-zone compartmental model, and found that the imperfect macro-mixing can broaden the molecular weight distribution (MWD) of LDPE. Based on the same three-zone model, Villa *et al.* [8] studied the effects of imperfect macro-mixing on the stability of LDPE reactors, and found that macro-mixing is important to the stability of LDPE reactors from time-scale comparisons of initiator half-lives and feed plume mixing times. Pladis and Kiparissides [2], and Yaghini and Iedema [3] proposed tank-in-series models to calculate the molecular weight and long chain branching distribution of the LDPE produced in autoclave reactors, and analyzed the effects of back-mixing on the MWD of LDPE products by varying the model parameters. Based on the aforementioned literature, the reactor stability and product properties have been predicted only considering the effects of macro-mixing [2,3,5–8]. Namely, it seems that the performance of LDPE autoclave reactors is controlled by the macro-mixing characteristics of fluid, and effects of the micro-mixing characteristics of fluid can be ignored.

However, some other researchers raised different opinions, and they believed that the effects of micro-mixing on the high-pressure polymerization of ethylene in LDPE autoclave reactors cannot be neglected. Smit [12] explained the minimum consumption of initiators based on a simplified micro-mixing model, and reproduced the lowest value of initiator consumption in a LDPE autoclave reactor. Tosun [13] researched the effects of micro-mixing on the number- and weight-averaged polymerization degree of LDPE in a semi-batch stirred tank by varying the dimensionless time constants θ_X, in which θ_X was estimated based on correlations of Pohorecki and Baldyga [14,15], and concluded that the weight-averaged polymerization degree is significantly affected by the micro-mixing characteristics of fluid in reactors, while the number-averaged polymerization degree is almost unaffected. Pladis and Kiparissides [16] proposed a dynamic segregation-back mixing model, and studied the effect of micro-mixing conditions on the initiator consumption in the LDPE autoclaves by varying the characteristic time of micro-mixing t_m, in which t_m was obtained from computational fluid dynamics (CFD) simulations and Corrsin's equations, and found that the micro-mixing characteristics of fluid in reactors can significantly affect the initiator consumption. As shown in these works, it was found that the micro-mixing characteristics of fluid in autoclave reactors may affect the consumption of initiators, and the molecular structure of LDPE products apparently. In other words, effects of the micro-mixing characteristics of fluid on the performance of LDPE autoclave reactors cannot be neglected [12,13,16].

In short, the contradiction still exists in publications, and one of the most significant is whether the micro mixing will affect the LDPE products. The contradiction may be caused by the following reasons. On one hand, most of them were conducted by the method of modelling, and the conditions of macro- and micro-mixing used in the models were arbitrarily given or obtained from CFD simulations and correlations [2,3,13,16], which means the results may be inaccurate for real LDPE autoclaves. On the other hand, the high-pressure polymerization of ethylene consists of a series of elementary reactions, but the researchers only focused on the effects of mixing on single or several elementary reactions [12,16], which led to the lack of a comprehensive understanding of the effects of macro- and micro-mixing on the high-pressure polymerization of ethylene in LDPE autoclaves.

In order to clarify which scale of mixing dominates the polymerization in the real LDPE autoclave reactor, a cold-flow LDPE autoclave was built to determine the macro-mixing and micro-mixing characteristics of fluid for a wide range of Reynolds number (*Re*) which covers the *Re* used in industry. Moreover, a sufficiently verified CFD simulation was conducted to explain the complex macro-mixing in this reactor. Finally, by comparing the characteristic times of macro-mixing, micro-mixing and various elementary reactions, the effects of macro-mixing and micro-mixing on the elementary reactions were revealed comprehensively, which is of great importance for the design, optimization and operation of LDPE autoclave reactors.

2. Experimental Apparatus and Methods

2.1. Macro-mixing experiment

The macro-mixing performance of a reactor refers to the macro-mixing characteristics of fluid in the reactor. Fig. 1 is a schematic diagram of the experimental apparatus to determine the macro-mixing characteristics of fluid in the LDPE autoclave reactor. The key part of the experimental apparatus, the stirred tank, is scaled down from an industrial autoclave reactor, which consists of a plexiglass tank with an inner diameter of 0.21 m and a height of 2.05 m, a ball bearing, a rolling bearing and a conical hopper with a top angle of 60°. Besides, it should be mentioned that compared with novel mixers, such as T-shaped and X-shaped micromixers [17,18], the autoclave reactor studied in this work has a complicated agitator with 32 impellers, which is driven by a motor. This feature contributes to the formation of specific flow fields and restricted end-end mixing in the LDPE autoclave reactor [19], which is conducive to produce the LDPE products with specific molecular structures, but increases the costs of the construction and operation of the reactor. Under the confidentiality requirement, details of the agitator cannot be given. In addition, compared with T-shaped and X-shaped micromixers, there is no surface with large curvatures on the wall of the autoclave reactor, which leads to that the reactor is not easily broken due to stress concentration under a high pressure.

The experimental apparatus also includes a storage tank, a centrifugal pump (IHG50-160, Shanghai Sunshine Pump, China), vortex flowmeters, tracer pulse injection systems, and a conductivity testing system. Each tracer pulse injection system consists of a U-shaped elbow pipe, a three-port valve and a ball valve. The tracer stored in U-shaped elbow pipes was injected into the pipelines by adjusting three-port valves and ball valves in the systems. Corresponding to the four inlets of the reactor (in0/in1/in2/in3, as shown in Fig. 1), there are also four tracer pulse injection systems installed along the axial direction of the reactor. The conductivity testing system mainly consists of the conductivity probes, the conductivity meter (DJS-1D, INESA, China, 1 $\mu S \cdot cm^{-1}$) and a computer. During the test, the conductivity probes were inserted into the reactor at different detection points p1/p2/p3/p4/p5/p6, and the insertion depth of the conductivity probes was 5 mm. The axial heights h/H of feeding points in0/in1/in2/in3 and conductivity detection points p1/p2/p3/p4/p5/p6 are shown in Table 1, which are consistent with the industrial LDPE autoclaves. The sampling frequency of the conductivity meter is 1 Hz, and the sampling time is set to 240 s.

The macro-mixing experiments were conducted under the pressure of 0.1 MPa, the temperature of 298 K. It should be noted here that the pressure and temperature of the experiments are quite different from those of real industrial LDPE reactors, and effects of these two parameters on the mixing characteristics of fluid are

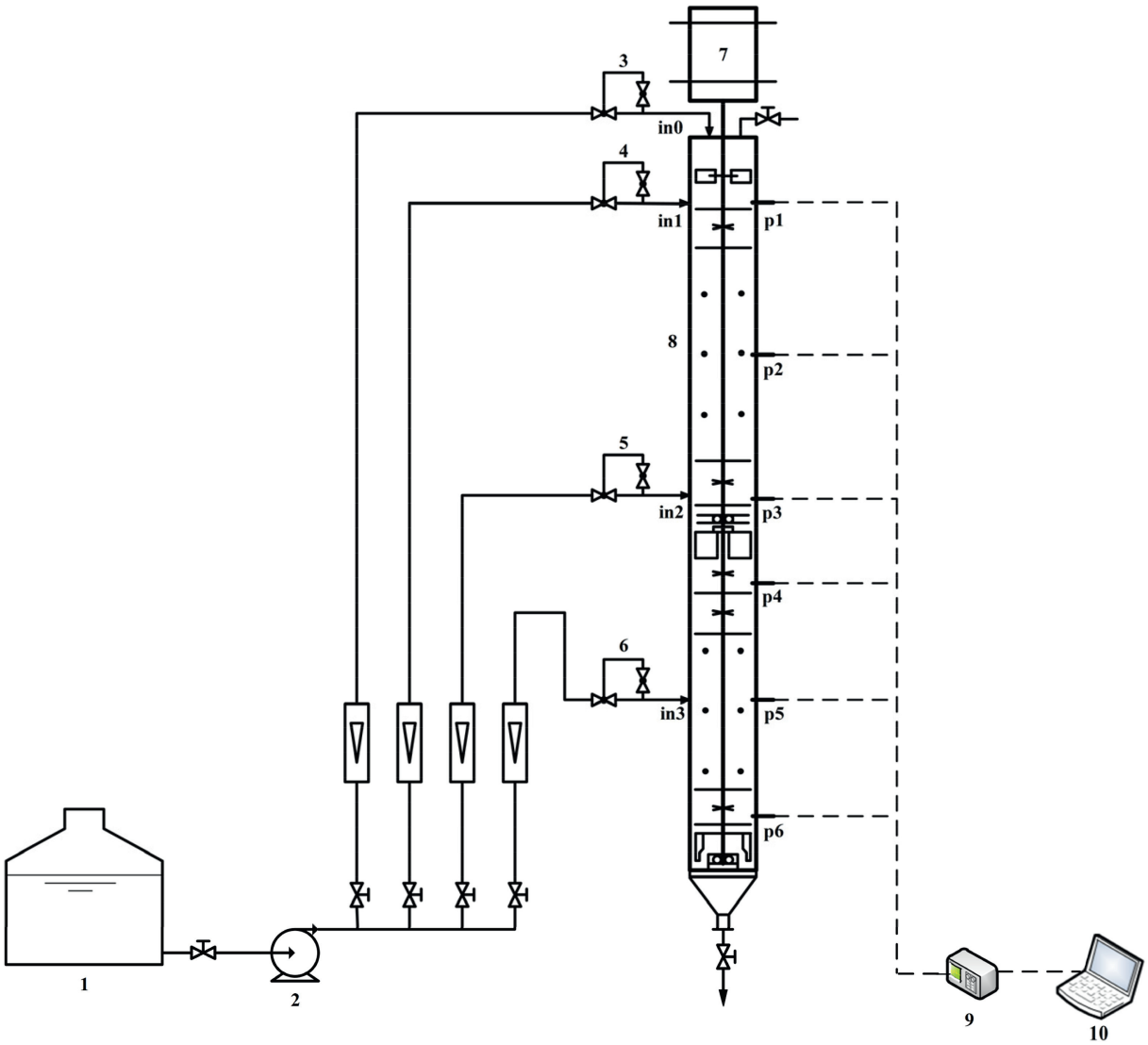

Fig. 1. Schematic diagram of experimental apparatus for the determination of macro-mixing characteristics of fluid in the LDPE autoclave reactor: (1) storage tank, (2) centrifugal pump, (3)–(6) tracer pulse injection systems, (7) motor, (8) stirred tank, (9) conductivity meter, (10) computer.

mainly reflected in the changes of the transport properties (*i.e.*, density, viscosity). During the experiments, the macro-mixing characteristics of fluid were determined by detecting the liquid conductivity response $\kappa(t)$ at different locations in the stirred tank after the electrolyte solution tracer was injected by pulse. Water ($\rho = 998\ \mathrm{kg\cdot m^{-3}}$, $\mu = 10^{-3}\ \mathrm{kg\cdot m^{-1}\cdot s^{-1}}$) was taken as the experimental fluid, and the NaCl solution with NaCl concentration of $8.78\ \mathrm{g\cdot L^{-1}}$ was selected as the tracer. The correlation between the liquid conductivity κ and the concentration of NaCl c is shown in Fig. 2. According to the published experimental investigations on agitated reactors, effects of the transport properties (*i.e.*, density, viscosity) on the macro-mixing characteristics of fluid are mainly dominated by the agitation Reynolds number *Re* [20–22]. Therefore, although the properties of water differ from those of reactants in the real LDPE reactor, the *Re* range (1.20×10^5–6.00×10^5) investigated in this work has been designed to cover the *Re* (1.45×10^5–2.68×10^5) in the real industry to provide a good support for industrial practice.

The macro-mixing measurement experiments were carried out through the following steps. Firstly, the tracer was added into the U-shaped elbow pipes, and the centrifugal pump was started until the stirred tank was filled with fluid. Secondly, the agitator rotation speed was slowly increased to $1000\ \mathrm{r\cdot min^{-1}}$ and kept for 3 min, then the rotation speed was gradually reduced to $0\ \mathrm{r\cdot min^{-1}}$ and kept static for 2 min to vent. The operation was repeated 2–3 times until there was no obvious bubble observed in the stirred tank. Thirdly, the agitator rotation speed was adjusted to the setting values (200–$1000\ \mathrm{r\cdot min^{-1}}$), and then the inlets and outlet of the stirred tank were opened and the flowrates of all feeds were adjusted to the setting values. It should be mentioned here that the volumetric flowrates at different feeding points are designed to ensure that the proportion of each feed to total feed and the mean residence time are consistent with those of the industrial LDPE reactor, as shown in Table 2. Finally, the three-port valves and ball valves in the pulse injection systems were adjusted to ensure that the tracer stored in U-shaped elbow pipes was injected into the feeds, and the conductivity data at various detection points was sampled.

The macro-mixing characteristics of fluid in reactors can be characterized by the residence time distribution (RTD), the macro-mixing time t_M and the mixing degree δ_m, *etc* [23–25]. In this work, the characteristic times of macro-mixing were investigated by the macro-mixing experiments, which were further compared with the characteristic time of elementary reactions to analyze the effects of fluid macro-mixing on the performance of the LDPE autoclave

Table 1
Locations of feeding points and conductivity detection points on the stirred tank.

Feeding points	h/H①	Conductivity detection points	h/H①
in0	1.000	p1	0.920
in1	0.920	p2	0.740
in2	0.550	p3	0.550
in3	0.260	p4	0.420
		p5	0.260
		p6	0.093

① h represents the height from the bottom of the plexiglass tank to these points, and H represents the height from the bottom of plexiglass tank to the height point in0.

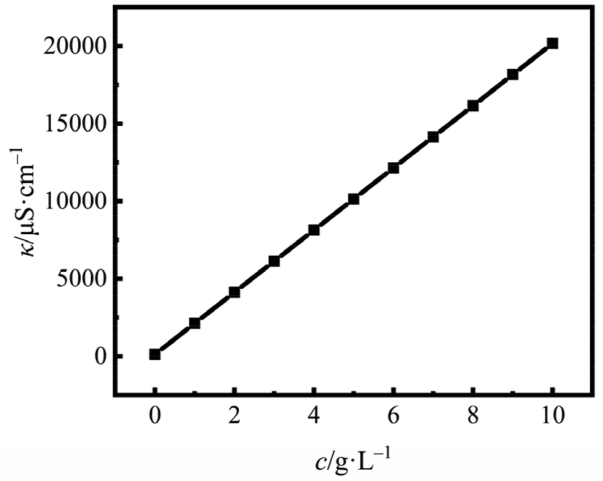

Fig. 2. Correlation between the conductivity and the concentration of NaCl in the solution.

Table 2
Volume flow rates of feeds.

Feeds	Feeding points	Volumetric flow rate $Q_{v,i}$/m^3·h^{-1}
inlet0	in0	0.854
inlet1	in1	1.720
inlet2	in2	1.720
inlet3	in3	1.720

reactor (see Section 4.3). The key is to select appropriate parameters as the characteristic times of fluid macro-mixing in the LDPE autoclave reactor.

In the Refs. [20,23], the t_M was generally selected as the characteristic time of fluid macro-mixing, which was defined as the time from the tracer releasing until the tracer concentration response $c(t)$ enters the 95% to 105% interval of the equilibrium concentration and then never escape the bounds. Here, it should be noted that this definition of t_M is only for batch-operated reactors, where the equilibrium concentration of tracer is constant. But for the LDPE autoclave reactor which is operated continuously, the aforementioned definition of t_M is not applicable due to the equilibrium concentration of tracer varying with the operating conditions and detection positions. To solve the problem, a new definition of t_M was proposed in this work, with reference to the aforementioned definition of t_M. In this new definition, the t_M at a certain position is the time from the tracer being step-injected until the tracer concentration reaches 95% of the equilibrium concentration at that position. Besides, based on the tracer concentration response at a certain position, it could also be found that the time from the tracer being step-injected until the tracer reaches that position cannot be neglected, which was named as the delay time t_d. To sum up, the t_d and the t_M with new definition were selected as the characteristic times of fluid macro-mixing in the LDPE autoclave reactor.

Since the LDPE autoclave reactor has a large height–diameter ratio ($H/D \approx 10$), the t_d and t_M may be different at different axial positions. Thus, as introduced in the above section, the tracer concentration response curve $c(t) \sim t$ was measured in different positions by pulse method, and in order to acquire the t_d and t_M, the pulse $c(t) \sim t$ curve was converted to $F(t) \sim t$ curve by Eq. (1). According to the $F(t)$ curve, the t_d at a specific detection position is the time required from tracer injection to $F(t)$ starting to rise, and the t_M at a specific detection position is the time taken for $F(t)$ to reach 0.95 since the tracer was injected, as shown in Fig. 3.

$$F(t) = \sum_{k=0}^{t} c(k) \Big/ \sum_{k=0}^{\infty} c(k) \tag{1}$$

2.2. Micro-mixing experiment

The micro-mixing performance of a reactor refers to the micro-mixing characteristics of fluid in the reactor. Fig. 4 is a schematic diagram of the experimental apparatus to determine the micro-mixing characteristics of fluid in the LDPE autoclave reactor. The stirred tank applied here shares the same structure as that in the macro-mixing experiment, and the axial heights h/H of acid injection points a1/a2/a3/a4, sampling points b1/b2/b3/b4/b5 are shown in Table 3. All of the acid injection pipe is flush with the inner wall of the reactor, which is consistent with the industrial LDPE reactor. Besides, the experimental apparatus includes a base solution storage tank (volume: 1 m^3), an acid storage tank (volume: 1 L), a centrifugal pump (IHG50-160, Shanghai Sunshine Pump, China), a peristaltic pump (BT100 N, Innofluid, China), and an ultraviolet spectrophotometer (UV-2102PC, UNICO, USA). Here, it is worthy to mention that the feeding points and detection points in micro-mixing experiments differ from those in the macro-mixing experiments. It is because the macro-mixing in a reactor is dominated by the circulation flow of fluid and turbulent diffusion, which is significantly affected by the feed conditions [26–28]. But the micro-mixing characteristics of fluid are mainly affected by transport properties (*i.e.*, density, viscosity) and turbulence dissipation

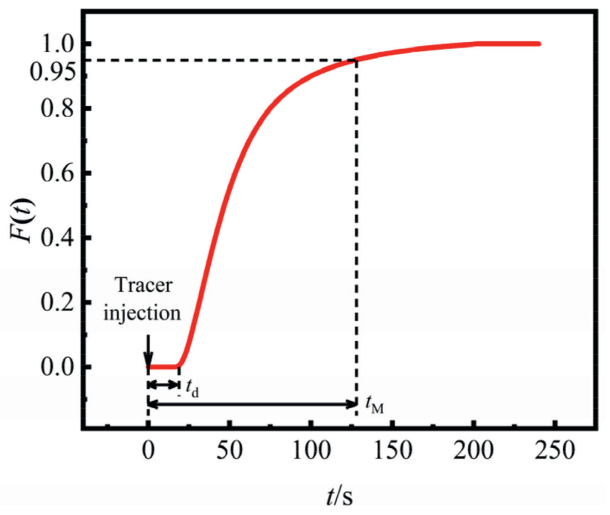

Fig. 3. The determination of delay time t_d and macro-mixing time t_M.

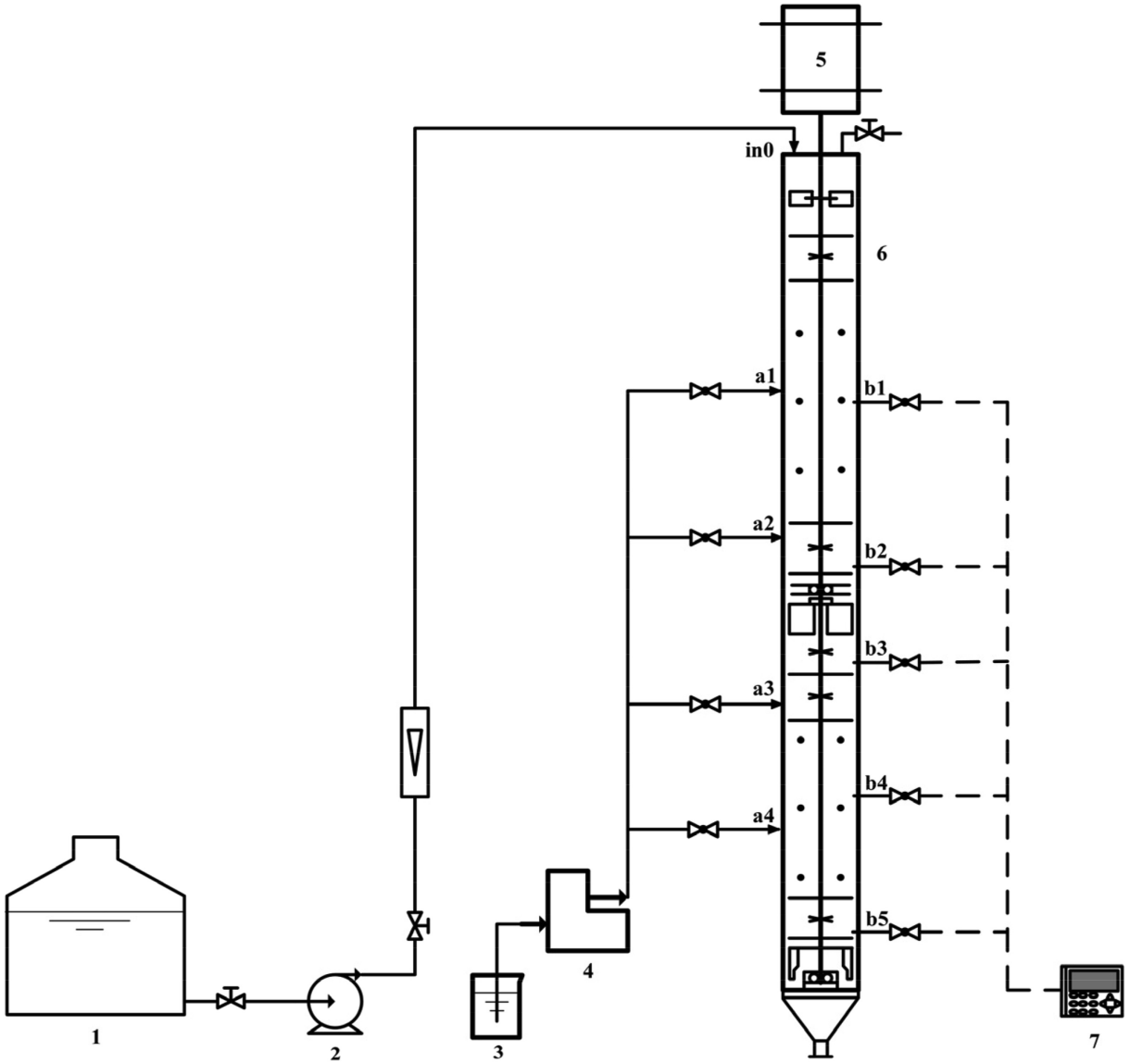

Fig. 4. Schematic diagram of experimental apparatus for the determination of the micro-mixing characteristics of fluid in the LDPE autoclave reactor: (1) base solution storage tank, (2) centrifugal pump, (3) acid storage tank, (4) peristaltic pump, (5) motor, (6) the stirred tank, (7) ultraviolet spectrophotometer.

Table 3
Locations of acid injection points and sampling points.

Acid injection points	*h*/*H*	Sampling points	*h*/*H*
a1	0.775	b1	0.750
a2	0.528	b2	0.555
a3	0.360	b3	0.415
a4	0.195	b4	0.250
		b5	0.085

rate of fluid [16,29,30], in which the turbulence dissipation rate of fluid is mainly affected by the intensity of agitation in the reactor, but little influenced by the feed conditions. In this work, the acid injection points and sampling points are almost uniformly arranged along the axial height of the reactor, as shown in Table 3, which aims to investigate the effects of the positions of these points on the results of micro-mixing experiments.

The micro-mixing experiments were also conducted under the pressure of 0.1 MPa, the temperature of 298 K. In the experiments, aqueous solutions with various mass fractions of glycerol were used, and the glycerol was used to regulate the viscosity and density and check if the *Re* can characterize the comprehensive effects of fluid transport properties (*i.e.*, density, viscosity) on the micro-mixing characteristics. The densities of aqueous solutions are 1000, 1051, 1085, 1098, 1114 $kg \cdot m^{-3}$, and the corresponding viscosities are 1.00×10^{-3}, 1.75×10^{-3}, 2.93×10^{-3}, 3.79×10^{-3}, 5.04×10^{-3} $kg \cdot m^{-1} \cdot s^{-1}$.

The measurement of the micro-mixing characteristics of fluid was based on the method of molecular probe-ultraviolet spectrophotometry. Although this method also depends on injecting a tracer into the reactor, but compared to the macro-mixing experiment (no reactions happen after injection), reactions are necessary. In previous works, some standard reaction systems have been proposed and widely used to determine the micro-mixing behavior in various kinds of reactors [31,32]. The Villermaux–Dushman reaction system is one of those standard reaction systems, which was selected in this work. Besides, it should be noted that micro-mixing in the reactor is just a physical process, which is independent of the

reaction kinetics, and the selected reaction system is just used as a tool to determine the micro-mixing characteristics of fluid in the reactor.

The Villermaux–Dushman reaction system consists of several reactions, as shown in Eqs. (2)–(4), where the rate of reaction (a) is much larger than that of reaction (b) [33,34]. The concentration of I_3^- in the product depended on the micro-mixing characteristics of fluid in the reactor, which could be determined by the ultraviolet spectrophotometer.

$$\text{Reaction (a)}: H_2BO_3^- + H^+ \xrightarrow{k_1} H_3BO_3 \tag{2}$$

$$\text{Reaction (b)}: 5I^- + IO_3^- + 6H^+ \xrightarrow{k_2} 3I_2 + 3H_2O \tag{3}$$

$$\text{Reaction (c)}: I_2 + I^- \overset{k_3}{\rightleftharpoons} I_3^- \tag{4}$$

It should be pointed out that micro-mixing in the reactor is a physical process, which is independent of the concentrations of reactants in the acid-base solutions. In this work, the concentrations of reactants were designed to be consistent with those in Rousseaux's experiments [35], which was for the convenience of the calculation of micro-mixing time t_m. Thus, the dilute sulfuric acid with the concentration of $c(H^+)_0 = 1\ mol\cdot L^{-1}$ was selected as the experimental acid, and the concentrations of H_3BO_3, NaOH, KI, KIO_3 in the base solution are shown in Table 4.

The micro-mixing experiments were carried out through the following steps. Firstly, the centrifugal pump was started, until the stirred tank was filled with the base solution. Secondly, the motor was started, and the variable-frequency driver was regulated to increase the agitator rotation speed to 700 $r\cdot min^{-1}$ slowly, and kept a constant stirring for 3 min. Then the rotation speed was gradually reduced to 0 $r\cdot min^{-1}$, and kept static for 2 min to vent. The operation was repeated 2–3 times until there was no obvious bubble observed in the stirred tank. Thirdly, the agitator rotation speed was adjusted to the setting values, then the peristaltic pump was started after 1 min, and the acid solution of 150 ml was slowly injected into the stirred tank. Here, it should be noted that the micro-mixing experiments aim to determine the quality of micro-mixing, which is independent of macro-mixing behavior in the reactor. However, the experimental results could be affected by the macro-mixing characteristics of fluid in the reactor when the flowrate of acid solution is too large, thus a proper flowrate of acid solution should be selected for the experiments. To solve the problem, several flowrates of the acid solution have been tried, and it was found that the experimental results were unaffected by the flowrate when its value is not greater than 3.57 $ml\cdot min^{-1}$. Thereby, the flowrate of acid solution was set to 3.57 $ml\cdot min^{-1}$. Finally, the fluid at points b1/b2/b3/b4/b5 was sampled, and the concentration of I_3^- in each sample was determined by the ultraviolet spectrophotometer.

Generally, the micro-mixing characteristics of fluid in reactors are characterized by the segregation index X_s and the micro-mixing time t_m [36]. The definition of X_s is shown in Eq. (5), where Y represents the ratio of the amount of H^+ consumed by reaction (b) to the amount of H^+ injected into the reactor, and Y_{TS} represents the value of Y in the case of complete segregation [33]. The values of Y and Y_{TS} could be calculated by Eqs. (6)–(9), where V_r and $V_{injection}$ represent the volumes of the reactor and the injected acid solution, respectively. $c(IO_3^-)_0$, $c(H_2BO_3^-)_0$ represent the concentrations of IO_3^-, $H_2BO_3^-$ in the base solution, respectively. $c(I^-)$, $c(I_2)$, $c(I_3^-)$ represent the concentrations of I^-, I_2, I_3^- in the samples, respectively. K_3 represents the equilibrium constant of reaction (c), and the value of K_3 equals to 700 at 298 K [37].

Table 4
Concentrations of components in the base solution.

Component	Molar concentration/$mol\cdot L^{-1}$
H_3BO_3	0.1820
NaOH	0.0909
KI	0.0117
KIO_3	0.0023

$$X_s = \frac{Y}{Y_{TS}} \tag{5}$$

$$Y = \frac{2[n(I_2) + n(I_3^-)]}{n(H^+)_0} = \frac{2V_r\cdot[c(I_2) + c(I_3^-)]}{V_{injection}\cdot c(H^+)_0} \tag{6}$$

$$Y_{TS} = \frac{6c(IO_3^-)_0}{6c(IO_3^-)_0 + c(H_2BO_3^-)_0} \tag{7}$$

$$c(I_2) + c(I_3^-) = \frac{3}{5}[c(I^-)_0 - c(I^-) - c(I_3^-)] \tag{8}$$

$$K_3 = \frac{c(I_3^-)\cdot c^\theta}{c(I_2)\cdot c(I^-)} \tag{9}$$

Compared with the segregation index X_s, the micro-mixing time t_m can characterize the quality of micro-mixing more intuitively, which was selected as the characteristic time of fluid micro-mixing in the LDPE autoclave reactor. However, the value of t_m could not be measured by experiments directly, and some models were proposed to calculate t_m, such as diffusion model, engulfment model, incorporation model, IEM model, *etc.* [38–40]. In this work, the incorporation model proposed by Villermaux [40] was used to calculate the micro-mixing volume ratio α, and the formula proposed by Rousseaux *et al.* [35] were chosen to calculate t_m, as shown in Eqs. (10) and (11).

$$\alpha = \frac{1 - X_s}{X_s} \tag{10}$$

$$t_m = \begin{cases} 0.73\alpha^{-2.26}, & 2 < \alpha < 5 \\ 0.82\alpha^{-2.30}, & 5 < \alpha < 7 \\ 0.15\alpha^{-1.45}, & 7 < \alpha < 20 \end{cases} \tag{11}$$

3. Simulation Method and Verification

3.1. Governing equations

The flow of fluid is governed by the continuity equation and momentum equations. According to the published literature [41], for the ethylene-LDPE mixtures with lower LDPE mass fraction ($w_{LDPE} \leq 22.5\%$), the correlation between the shear stress and the shear rate is almost linear within a wide range of shear rate (0–1200 s^{-1}), thus the fluid in the LDPE autoclave reactor can be assumed as a Newtonian fluid during the CFD simulations. Besides, the temperature rise due to viscous dissipation is assumed to be negligible. Therefore, the flow of fluid in the reactor can be described by the simplified continuity equation and momentum equations [42,43], as shown in Eqs. (12) and (13), where u_i is the component of velocity in dimension i, x_i is the component of coordinate in dimension i, p is the pressure, ρ is the density, and υ is the kinematic viscosity. In this work, water at 298 K was selected as

simulated fluid, and the values of ρ, υ are 998 kg·m^{-3} and 10^{-6} m^2·s^{-1} respectively.

Continuity equation:

$$\frac{\partial u_i}{\partial x_i}=0 \tag{12}$$

Momentum equation:

$$\frac{\partial u_i}{\partial t}+\frac{\partial (u_i u_j)}{\partial x_j}=-\frac{1}{\rho}\frac{\partial p}{\partial x_i}+\nu\frac{\partial^2 u_i}{\partial x_j^2} \tag{13}$$

In the mixing process, the mass fraction of tracer is governed by Eqs. (14)–(16), where Y_m is the mass fraction of species m, $J_{m,i}$ is the diffusion flux of species m in dimension i, and S_m is the source term of species m due to chemical reactions, $D_{m,i}$ is the molecular diffusivity of m in dimension i, Sc_t is the turbulent Schmidt number, μ_t is the turbulent viscosity, D_t is the turbulent diffusivity [26].

$$\frac{\partial}{\partial t}(\rho Y_m)+\frac{\partial}{\partial x_i}(\rho\cdot u_i\cdot Y_m)=-\frac{\partial}{\partial x_i}J_{m,i}+S_m \tag{14}$$

$$J_{m,i}=-\left(\rho D_{m,i}+\frac{\mu_t}{Sc_t}\right)\nabla Y_m \tag{15}$$

$$Sc_t=\frac{\mu_t}{\rho D_t} \tag{16}$$

In the case of turbulent flow, the method of Reynolds-averaged was used to solve Eq. (13), based on the average velocities and the fluctuating terms. Because of features cited in the literature [4], the turbulence model of renormalization group (RNG) k–ε was adopted to approximate the Reynolds stress term in this work.

3.2. Numerical solution

In the steady simulations of flow field in the LDPE autoclave reactor, the multiple reference frame (MRF) method was adopted to solve Eq. (13). The velocity fields were obtained until the total normalized residuals were not greater than 10^{-5}. Moreover, the velocity magnitudes at the conductivity detection points p1–p6 were set as indicators to determine the convergence. After the flow was fully established, the sliding mesh method was selected to simulate the movement and distribution of the tracer in the reactor. Due to the evolution of tracer concentrations being transient, it requires time-dependent calculations, and the time step was set to 1.0×10^{-4} s. During each time step, the calculations were completed until the residual of tracer mass fraction was not greater than 10^{-6}.

Based on the finite-volume method, the simulations of the LDPE autoclave reactor were conducted by using the CFD package of Fluent 19.0 (Ansys Inc.). The molecular diffusivity D_m was set to the value of 2.88×10^{-9} m^2·s^{-1}. The pressure–velocity coupling scheme was set to SIMPLE. The discretization scheme of turbulent kinetic energy, turbulent dissipation rate was set to first order upwind, and that of other terms (pressure, momentum, *etc.*) was set to second order upwind. The geometry of the computational fluid region is identical to that mentioned in the macro-mixing experiment, where the agitator regions ($h/H > 0.52$, $h/H < 0.51$) were defined as rotating zones, and the middle bearing regions ($0.51 \le h/H \le 0.52$) were defined as stationary zones. Besides, in order to obtain the mesh-independent solutions, different mesh sizes were tested (shown in Fig. 5), and the mesh with the grid number of 5.57×10^6 was adopted in the simulations eventually.

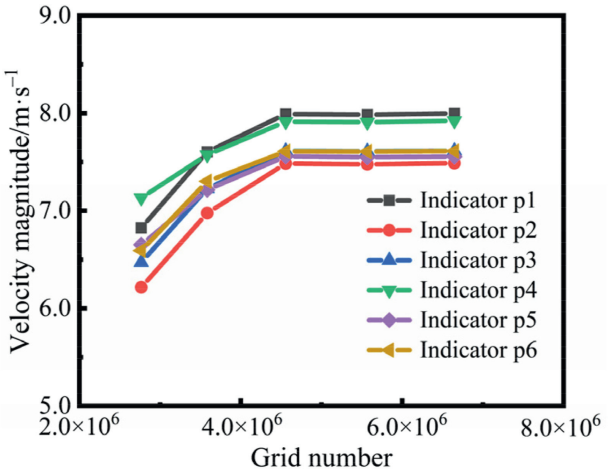

Fig. 5. Grid independence test.

3.3. Simulation verification

The CFD simulations were conducted at the agitator rotation speeds of 200, 400, 600, 800 and 1000 r·min^{-1}. Before the further analysis of simulation results, it is necessary to verify the accuracy, thus the velocity experiment was carried out, and water (298 K) was taken as the experimental medium. The axial velocities u_a, radial velocities u_r, and tangential velocities u_t at various positions were measured by Pitot tubes and a differential-pressure transmitter in the cold-flow experimental apparatus (shown in Fig. 1). The locations of detection points are shown in Table 5. Volumetric flow rates of all the feeds are given in Table 2.

At the agitator rotation speed of 1000 r·min^{-1}, the simulated result of velocity field is given in Fig. 6, and the comparison of experimental and simulated values of velocity components at different detection points is shown in Fig. 7. Due to the circulation flow caused by the turbine impellers, it can be observed that the direction of u_a at the positions near the shaft ($r/R = 0.38$) is upward, and that at the positions near the wall ($r/R = 0.91$) is downward. The farther away from the turbine impeller, the weaker the circulation flow, thus the u_a at the positions ($h/H = 0.42, 0.92$) near the turbine impellers are greater than that at the positions farther away. Since the turbine impellers are radial flow agitators, the radial flow nearby is stronger than that at other positions. The values of u_r at the positions near the turbine impellers ($h/H = 0.42, 0.92$) are obviously greater than those at other positions. Besides, the direction of radial flow is away from the shaft, and the values of u_r at the positions near the shaft ($r/R = 0.38$) are greater than those at the positions near the wall ($r/R = 0.91$). Moreover, the impellers in the reactor have almost the same diameter, thus the values of tangential velocities u_t at different axial heights are similar. Besides, the direction of tangential flow is identical to that of agitator rotation, and the values of u_t at the positions near the shaft ($r/R = 0.38$) are obviously less than those at the positions near the wall ($r/R = 0.91$).

Table 5
Locations of velocity detection points.

Detection points	h/H	r/R[①]
v1, v11	0.920	0.380, 0.910
v2, v21	0.740	0.380, 0.910
v3, v31	0.550	0.380, 0.910
v4, v41	0.420	0.380, 0.910
v5, v51	0.260	0.380, 0.910
v6, v61	0.093	0.380, 0.910

[①] r represents the distance from the centerline of the agitator shaft to these points, and R represents the inner radius of the plexiglass tank.

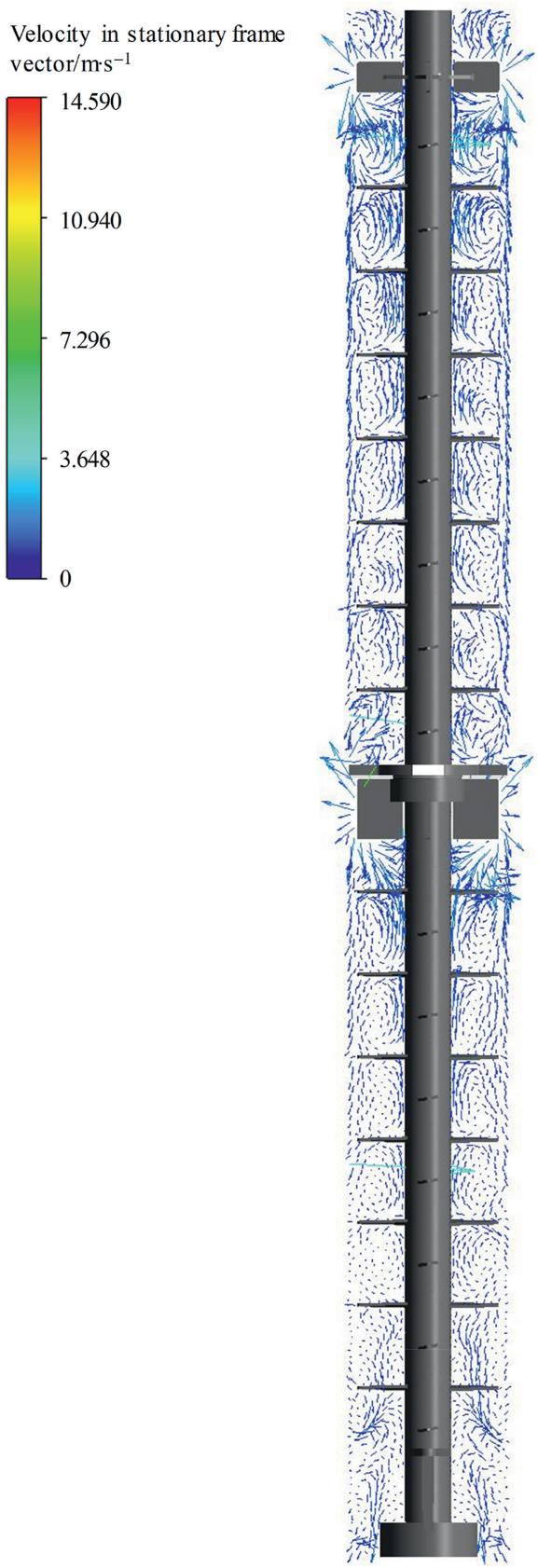

Fig. 6. The simulated results of velocity field in the stirred tank (N = 1000 r·min^{-1}, ρ = 998 kg·m^{-3}, μ = 10^{-3} kg·m^{-1}·s^{-1}).

Meanwhile, it can be found that the experimental and simulated velocities at various detection points are in good agreement, and the relative deviations of both values are less than 12.5%, as shown in Fig. 7. Consequently, it can be concluded that the simulation results of flow fields in the LDPE autoclave are credible.

4. Results and Discussion

4.1. Macro-mixing characteristics

The macro-mixing characteristics of fluid in a stirred tank are closely related to its transport properties (ρ, μ), impeller diameter d and agitator rotation speed N. The Re was widely used to characterize the comprehensive effect of all these factors on the macro-mixing characteristics of fluid in a stirred tank, whose definition was given in Eq. (17) [20–22].

$$Re = \frac{d^2 \cdot (N/60) \cdot \rho}{\mu} \tag{17}$$

Due to the large height–diameter ratio ($H/D \approx 10$) and the complicated structure of the agitator, the macro-mixing state at different positions in the LDPE autoclave may differ significantly. Besides, multiple feeds exist along the axial direction of the LDPE autoclave, thus the macro-mixing characteristics of different feeds may be different. Therefore, the effects of Re on the t_d, t_M at different axial positions (p1–p6) were investigated for each feed, within a wide range of $Re = 1.20 \times 10^5$–6.00×10^5.

Under different agitation Re, five macro-mixing experiments were conducted. Fig. 8 gives the delay time t_d for each feed at different axial positions. As shown in Fig. 8, the t_d at the positions near the feeding point is less than that at the positions farther away from the feeding point for each feed. This is mainly due to that the feeds mingle with the surrounding fluid constantly along the flow path, and it takes more time for them to reach the farther positions. Meanwhile, as Re increases, the t_d at different axial positions decreases, and the difference among t_d at the various positions also decreases. This indicates the macro-mixing is enhanced by increasing the Re, which may be caused by the variation in the degree of circulation flow.

In order to further reveal how the macro-mixing is enhanced as Re increases, one transient-state simulation and five steady-state simulations were performed. Fig. 9 gives the concentration distribution of tracer inside the reactor at different moments when the tracer was injected from inlet2 and inlet3 ($Re = 3.60 \times 10^5$). It can be clearly observed that the tracer undergoes a circulation flow in the reactor. Namely, the tracer injected at the middle part of the reactor will first flow to the upper part of the reactor and then go back to the lower part, and macro-mixing occurs during this circulation flow. Therefore, the key point to reveal the effect of Re on the macro-mixing is to demonstrate the variation of circulation flow with the increasing Re.

Based on the velocity fields obtained by the steady simulations, the circulation flow ratio R_c was proposed to quantify the degree of circulation flow in the LDPE autoclave reactor, whose definition is shown in Eq. (18), where $Q_{v,up}$, $Q_{v,down}$ represent the volumetric flowrates of upward and downward flow through a cross-section respectively. Fig. 10 gives the circulation flow ratio R_c at different Re. As shown in Fig. 10, when $Re > 2.40 \times 10^5$ and $h/H < 0.8$, the circulation flow ratio R_c reaches the maximum value when $h/H = 0.45$. This is mainly due to the strong suction and discharge capabilities of the 4-blade turbine located near the position of $h/H = 0.45$, and the circulation flow in the vicinity is stronger than that in other areas. Besides, along with the increase of Re, the

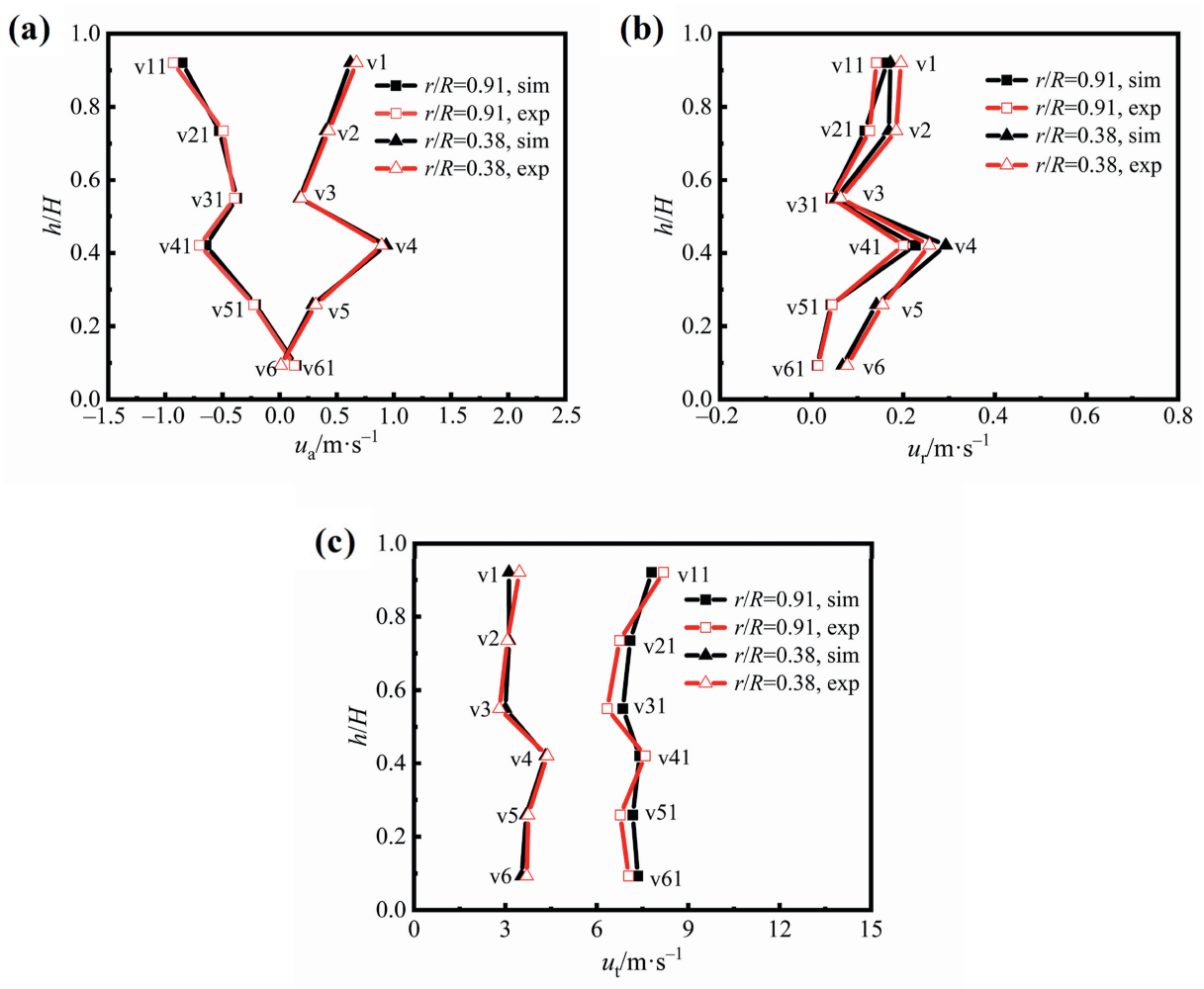

Fig. 7. The comparison of experimental and simulated values of velocity components at detection points: (a) axial velocities, (b) radial velocities, (c) tangential velocities.

circulation flow ratios R_c at different h/H increase, which indicates that the degree of circulation flow in the reactor increases as *Re* increases, then the macro-mixing is enhanced accordingly. Thus, along with the increase of *Re*, it takes less time for each feed to reach different positions p1–p6, and the times required to reach these positions tend to be identical.

$$R_c = \frac{Q_{v,up}}{Q_{v,down} - Q_{v,up}} \tag{18}$$

Fig. 11 gives the macro-mixing time t_M for each feed at different axial positions. As shown in Fig. 11, the t_M for feeds inlet0 and inlet1 are almost identical at the same axial position, which differ from those for feeds inlet2 and inlet3. This is mainly due to the locations of in0 and in1 are close, and both of them locate at the top of the reactor.

For feeds inlet0 and inlet1, which enter at the top part of the autoclave, Fig. 11(a) and (b) show that variations of the t_M with *Re* in the regions above the middle bearing (p1, p2, p3) and below that (p4, p5) are quite different. Along with the increase of *Re*, the t_M for feeds inlet0, inlet1 at p1, p2, p3 increases, but that at p4, p5 decreases. It is because that the circulation flow in the upper zone ($h/H > 0.52$) of the reactor is apparently strengthened with the increase of Re (See Fig. 10), which leads to the feeds inlet0, inlet1 staying in the upper zone ($h/H > 0.52$) for longer times, and the times required for the tracer concentrations at p1–p3 to reach the equilibrium values increase accordingly. Besides, in the lower zone ($h/H < 0.51$) of the reactor, the feeds inlet0, inlet1 mainly flow through the region near the wall. As *Re* increases, the downward flow in the region near the wall is strengthened, which leads to the feeds inlet0, inlet1 staying in the lower zone ($h/H < 0.51$) for shorter times, and the times required for the tracer concentrations at p4, p5 to reach the equilibrium values decrease accordingly.

For feeds inlet2 and inlet3, which enter at the middle part of the autoclave, Fig. 11(c) and (d) show that the t_M at different axial positions (p1–p6) increases as *Re* increases, and the t_M at the positions near feeding points are apparently less than that at the positions farther away. This is mainly due to that the feeds mingle with the surrounding fluid constantly along the flow path, thus it takes longer times for them to achieve the stable concentration at the farther positions. Besides, along with the increase of *Re*, the circulation flows in both the upper and lower zones are strengthened (see Fig. 10), which leads to the feeds inlet2, inlet3 staying in these two zones for longer times, and the times required for the tracer concentrations at p1–p6 to reach the equilibrium values increase.

Furthermore, Fig. 11 also shows that under any conditions, the t_M at different axial positions always tend to be identical along with the increase of *Re*. This is because the degree of non-ideal mixing in the autoclave decreases as *Re* increases, and the flow pattern of the whole autoclave approximates to ideal mixed flow at higher *Re*.

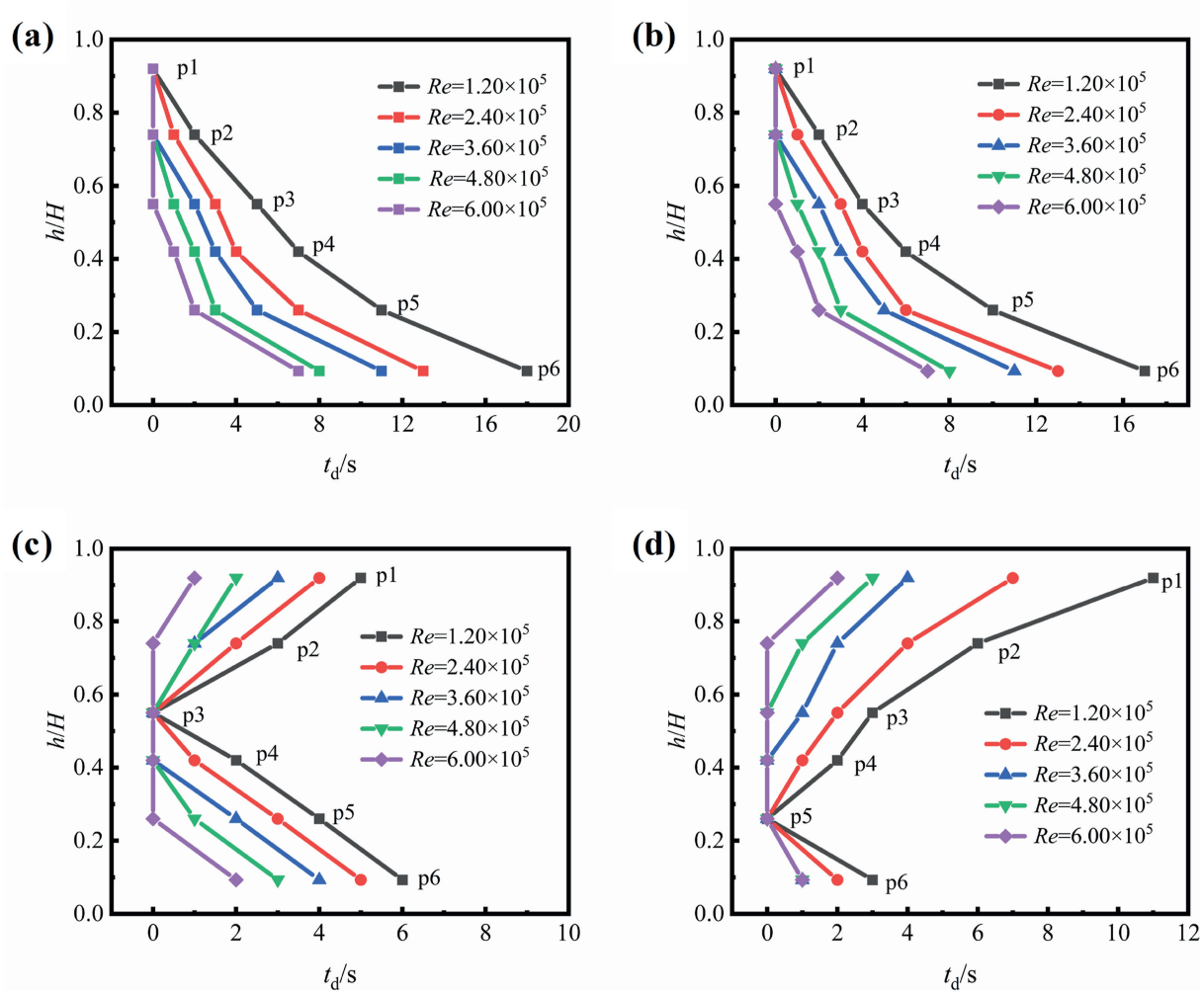

Fig. 8. The delay times t_d for each feed at different axial positions: (a) inlet0, (b) inlet1, (c) inlet2, (d) inlet3.

4.2. Micro-mixing characteristics

The quality of micro–mixing depends on the transport properties and turbulence dissipation rate of fluid [44,45]. For the LDPE autoclave, due to the large height-diameter ratio ($H/D \approx 10$), the variation of the micro-mixing characteristics of fluid along the axial height should be considered. However, it should also be considered that most of the impellers share the same structure, and are closely arranged in the LDPE autoclave, which leads to the turbulence conditions at different axial positions being similar. Thereby, it could be assumed that the difference in the micro-mixing characteristics at different axial positions is small. In order to further verify the correctness of the assumption, fourteen pre-experiments were conducted.

During the pre-experiments, the micro-mixing characteristics at different sampling points (b1–b5) were investigated at the conditions of $\upsilon = 10^{-6}\ m^2 \cdot s^{-1}$ and $N = 300\ r \cdot min^{-1}$, after the acid solution was injected at a2, a4 separately. The experimental results showed that the X_s and t_m at different h/H are similar, as shown in Fig. 12, and the maximum relative deviations of X_s, t_m at these sampling points (b1–b5) are less than 6% and 8% respectively. Namely, the difference in micro-mixing characteristics at different axial positions can be neglected. For the convenience of further research, the $\overline{X_s}$ and $\overline{t_m}$ of the reactor could be proposed, which were defined as the arithmetic average values of X_s, t_m at different sampling points b1–b5.

In addition, the effects of the axial position of the acid injection point on the $\overline{X_s}$ and $\overline{t_m}$ were also investigated at the conditions of $\upsilon = 10^{-6}\ m^2 \cdot s^{-1}$ and $N = 300\ r \cdot min^{-1}$, during the pre-experiments. As shown in Fig. 13, both the $\overline{X_s}$ and $\overline{t_m}$ vary little after the acid solution was injected at different points a1–a4, and the maximum relative deviations of $\overline{X_s}$, $\overline{t_m}$ are less than 3% and 5%, respectively. Namely, the effects of the axial position of the acid injection point on the experimental results can also be neglected.

As reported in the literature [44,45], the quality of micro-mixing is correlated to the size of the smallest fluid vortex mass λ_k, and better homogenization on the molecular scale can be achieved as λ_k decreases. The definition of λ_k is shown in Eq. (19), where ε represents the turbulence dissipation rate of fluid, and λ_k decreases with the increase of ε and the decrease of υ. In the LDPE autoclave, the turbulence dissipation rate ε is closely related to the agitator rotation speed N, and ε increases with the increase of N, under the same kinematic viscosity υ.

$$\lambda_k = \left(\frac{\upsilon^3}{\varepsilon}\right)^{1/4} \tag{19}$$

Consequently, the $\overline{X_s}$ and $\overline{t_m}$ of the LDPE autoclave reactor are significantly affected by the kinematic viscosity and agitator rotation speed. In this work, thirteen micro-mixing experiments were conducted to investigate the effects of υ, N on the $\overline{X_s}$ and $\overline{t_m}$, as

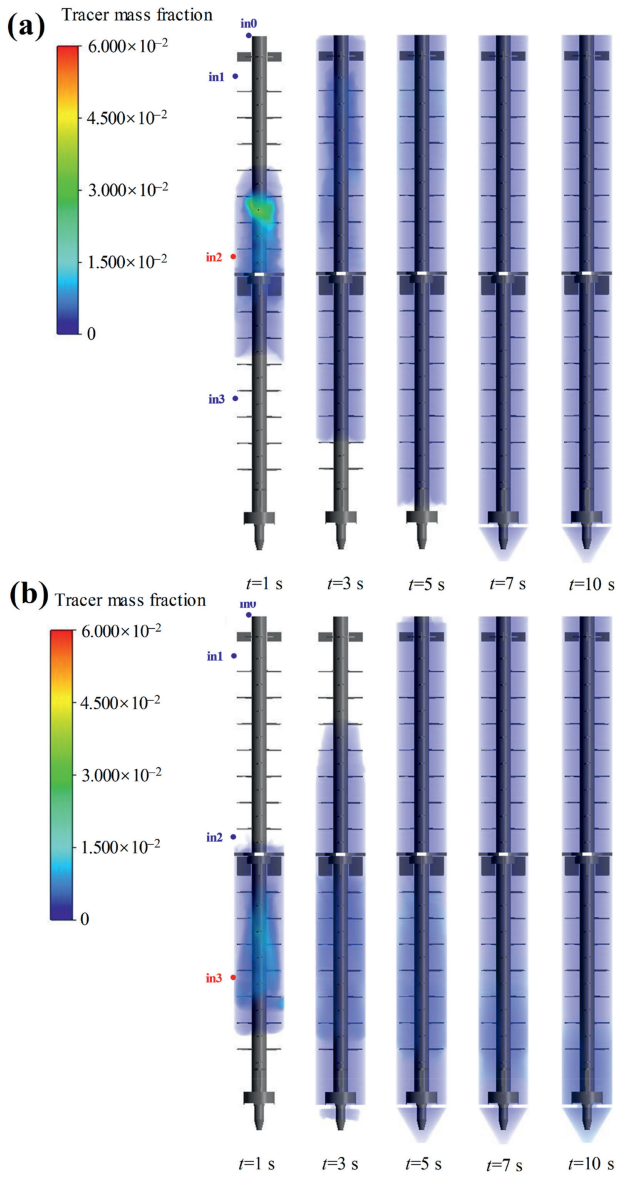

Fig. 9. The concentration distributions of tracer in the reactor at different moments ($Re = 3.60 \times 10^5$): (a) tracer was injected into the feed inlet2, (b) tracer was injected into the feed inlet3.

shown in Table 6. Experimental results in the table showed that both the $\overline{X_s}$ and the $\overline{t_m}$ increase as υ increases, and decrease with the increase of N. This is mainly due to the decrease of λ_k is conducive to the molecular diffusion on the microscopic scale, and the quality of micro-mixing increases accordingly.

As shown above, the definition of Re contains both the terms of υ ($\upsilon=\mu/\rho$) and N. Therefore, the Re is used to unify the effects of υ, N, and the effect of Re on the micro-mixing characteristics is shown in Fig. 14. It can be concluded that Re can characterize the comprehensive effects of υ and N on the micro-mixing characteristics of fluid in the LDPE autoclave, and both $\overline{X_s}$, $\overline{t_m}$ decrease with the increase of Re. The correlations between $\overline{X_s}$, $\overline{t_m}$ and Re can be given in the form of power functions, as shown in Eqs. (20) and (21), where the unit of $\overline{t_m}$ is s.

$$\overline{X_s} = \frac{230}{Re^{0.646}} \tag{20}$$

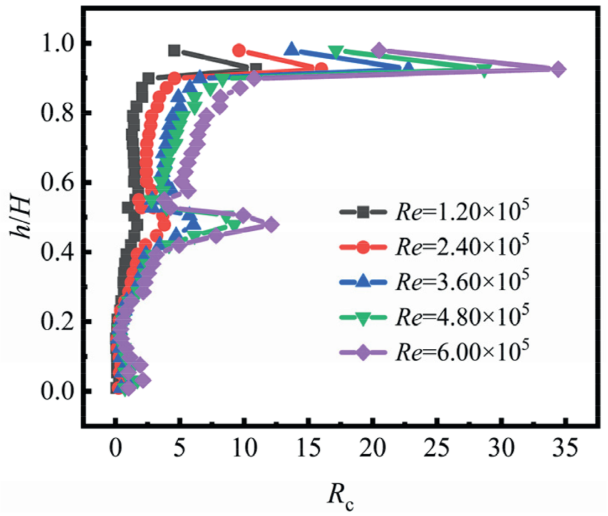

Fig. 10. The circulation flow ratio R_c at different Re.

$$\overline{t_m} = \frac{78261}{Re^{1.354}} \tag{21}$$

Moreover, it should be mentioned that the cold-flow reactor differs from the industrial LDPE autoclave in size, thus if Eq. (21) can also be used to the industrial autoclave reactors needs further verification. Here, the CFD simulation which has been validated above is used to acquire the $\overline{t_m}$ in an industrial reactor. Based on the CFD simulation, the turbulence dissipation rate ε is acquired and the $\overline{t_m}$ can be calculated by the Engulfment model, as shown in Eq. (22) [16]. Under a typical condition (ρ = 480 kg·m^{-3}, $\mu = 7.00 \times 10^{-3}$ kg·m^{-1}·s^{-1}, Re = 2.26×10^5) used in industry, the value of $\overline{t_m}$ calculated by Eq. (22) is 0.00498 s, and the relative deviation between this value and the value calculated from Eq. (21) is only 13%. Thereby, it could be concluded that Eq. (21) is also applicable to the industrial LDPE autoclave reactor.

$$t_m = 17.3\sqrt{\frac{\upsilon}{\varepsilon}} \tag{22}$$

4.3. Effects of macro-mixing and micro-mixing on elementary reactions

In this section, effects of macro- and micro-mixing on the polymerization will be comprehensively analyzed by comparing the characteristic times of macro-mixing (t_d, t_M), micro-mixing ($\overline{t_m}$) and elementary reactions within the industrial range of Re. Here, the industrial range of Re is determined as follows. According to the literature [46], the viscosity of ethylene-LDPE mixture (μ_m) in the LDPE autoclave reactor is in the range of 7×10^{-3}–1×10^{-2} kg·m^{-1}·s^{-1}, within the industrial operating conditions. The density of ethylene-LDPE mixture (ρ_m) is in the range of 440–570 kg·m^{-3}. Thereby, the range of Re is 1.45×10^5–2.68×10^5.

Based on experimental results in Section 4.1, when Re is in the range of 1.45×10^5–2.68×10^5, the corresponding ranges of t_d, t_M are 0–17 s and 22–107 s respectively, as shown in Table 7. Besides, the range of $\overline{t_m}$ can be obtained by Eq. (21) in Section 4.2, which is 3.50×10^{-3}–8.04×10^{-3} s.

As to the characteristic times of elementary reactions under industrial conditions (423–553 K, 130–250 MPa), they can be calculated by the formula proposed in the literature [16]. Here, it should be noted that numerous initiators are used in the industry to

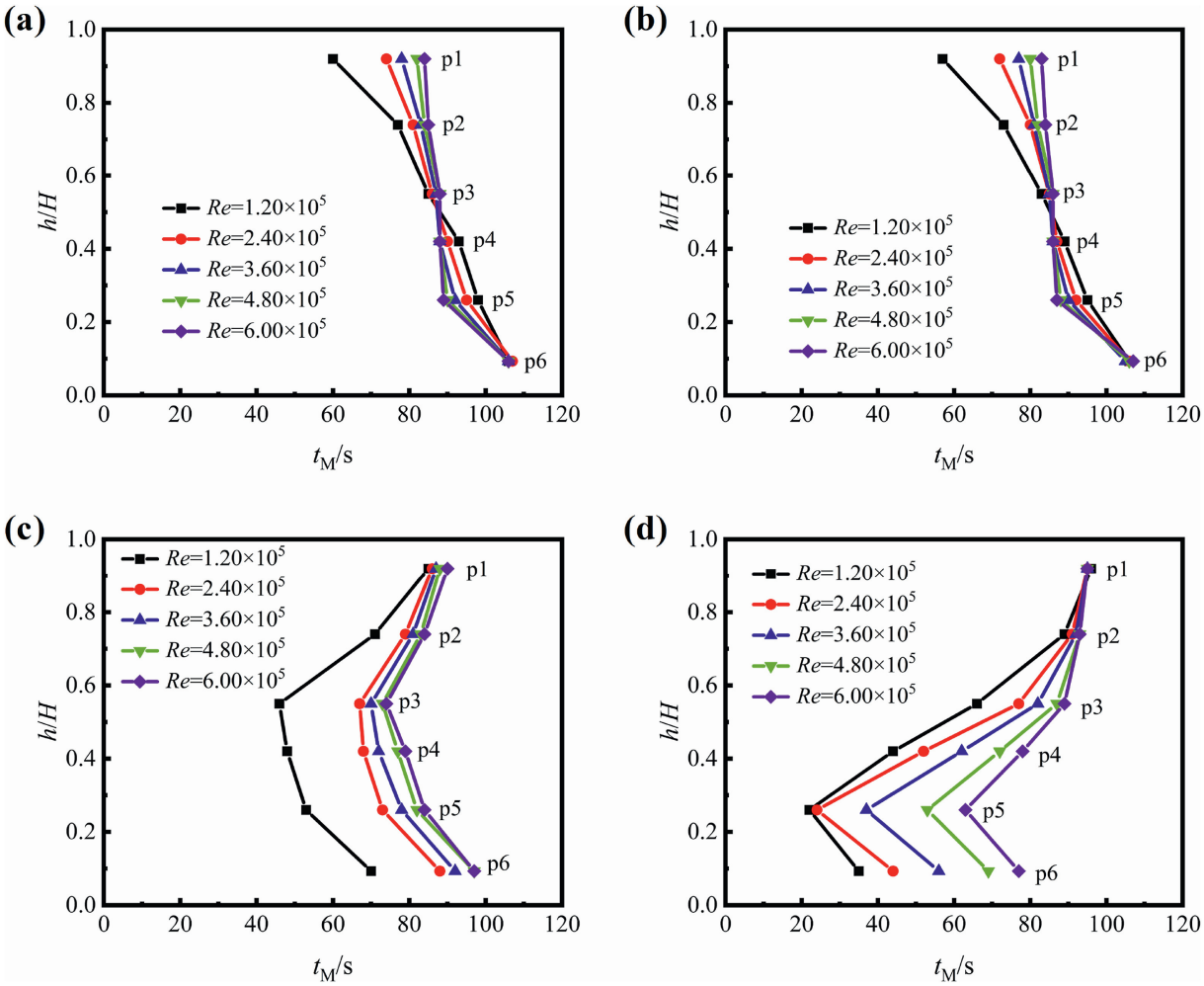

Fig. 11. The macro-mixing time t_M for each feed at different axial positions: (a) inlet0, (b) inlet1, (c) inlet2, (d) inlet3.

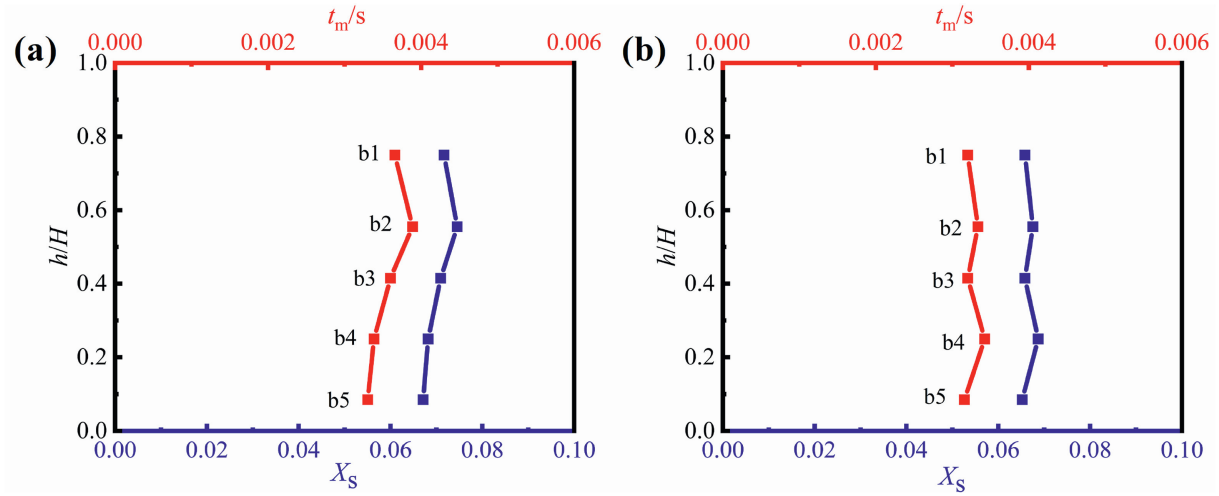

Fig. 12. The micro-mixing characteristics at different sampling points (b1, b2, b3, b4, b5): (a) acid injection at a2, (b) acid injection at a4.

cover a wide reaction temperature. For simplification, just three initiators TBPND, TBPO and TBPB are evaluated. The corresponding operating temperature ranges of these three initiators are 423–453, 453–503 and 503–553 K respectively, which almost cover the whole possible operation temperatures in the industry. The reaction kinetics of various elementary reactions used to calculate characteristic times of elementary reactions are given in Tables 8 and 9 [2].

In addition, $[R_0]$ and λ_0, which represent the concentration of primary radical and the zero-order moment of radical

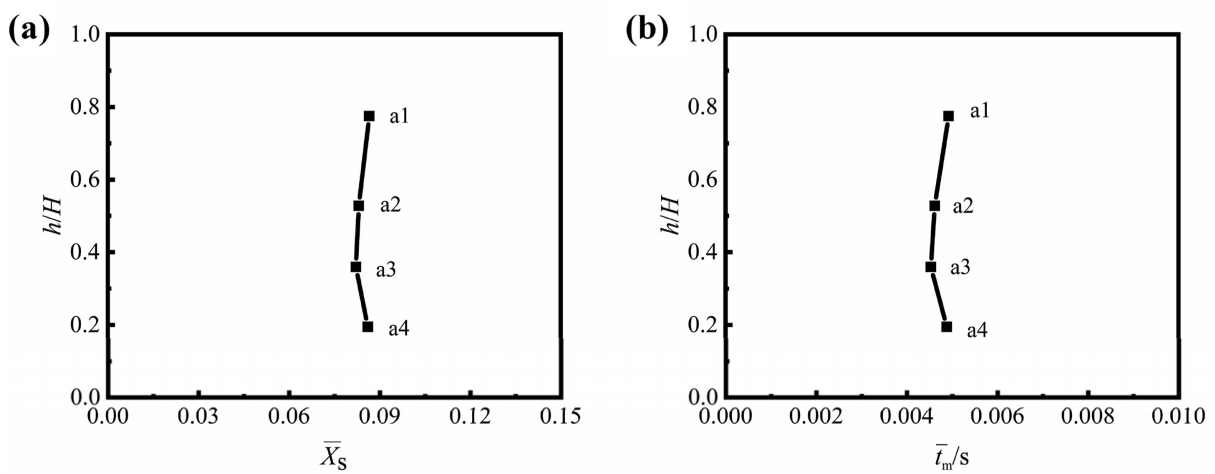

Fig. 13. The effects of the axial position of the acid injection point on the $\overline{X_s}$, $\overline{t_m}$: (a) average segregation index $\overline{X_s}$, (b) average micro-mixing time $\overline{t_m}$.

Table 6
The $\overline{X_s}$, $\overline{t_m}$ under different conditions.

N/r·min^{-1}	ρ/kg·m^{-3}	$\mu \times 10^3$/kg·m^{-1}·s^{-1}	$Re \times 10^{-4}$	$\overline{X_s}$	$\overline{t_m}$/s
300	1000	1.00	18.00	0.0872	0.00498
300	1051	1.75	10.80	0.138	0.0121
300	1085	2.93	6.68	0.182	0.0244
300	1098	3.79	5.23	0.207	0.0351
300	1114	5.04	3.99	0.225	0.0446
400	1000	1.00	24.10	0.0718	0.00367
400	1051	1.75	14.50	0.123	0.00869
400	1085	2.93	8.91	0.155	0.0166
400	1098	3.79	6.97	0.174	0.0216
400	1114	5.04	5.32	0.194	0.0292
350	1000	1.00	21.10	0.0780	0.00418
500	1000	1.00	30.10	0.0657	0.00319
600	1000	1.00	36.10	0.0602	0.00279

concentration, are needed during the calculation. With the steady-state approximation method, the values of [R_0] and λ_0 can be obtained by Eqs. (23) and (24), where [I], [M] represent the concentrations of initiator, monomer respectively, with the unit of kmol·m^{-3}. The initiator decomposition efficiency f was set to 0.7.

$$\lambda_0 = \sum_{n=1}^{\infty} [R_n] = \left(\frac{2f \cdot k_d [I]}{k_{td} + k_{tc}}\right)^{0.5} \tag{23}$$

Table 7
The overall ranges of t_d and t_M at different detection points.

Detection points	Axial height	t_d/s		t_M/s	
	h/H	min	max	min	max
p1	0.920	0	10	60	93
p2	0.740	1	6	74	87
p3	0.550	0	5	53	86
p4	0.420	1	6	48	92
p5	0.260	0	10	22	94
p6	0.093	2	17	37	107

Table 8
Reaction kinetics of initiator decomposition.

Initiators	Equation	k_0/s^{-1}	E_a/J·kmol^{-1}
TBPND		1.52×10^{14}	1.15×10^8
TBPO		1.54×10^{14}	1.25×10^8
TBPB	$I \xrightarrow{k_d} 2R_0$	2.23×10^{16}	1.52×10^8

$$[R_0] = \frac{2k_d \cdot [I]}{k_i \cdot [M]} \tag{24}$$

The values of [M] can be estimated by Eqs. (25)–(29), where ρ_E, ρ_{LDPE} and ρ_m represent the density of ethylene, LDPE and the

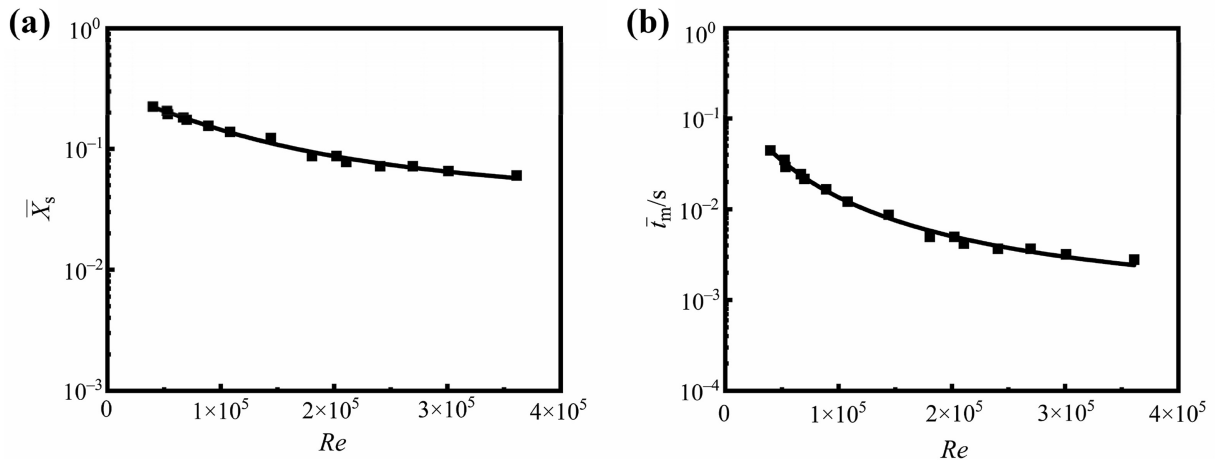

Fig. 14. The effects of Re on the micro-mixing characteristics in the stirred tank: (a) average segregation index $\overline{X_s}$, (b) average micro-mixing time $\overline{t_m}$.

Table 9
Reaction kinetics of chain initiation, chain propagation, chain transfer and chain termination.

Elementary reactions	Equations	k_0 /kmol^{-1}·m^3·s^{-1}	E_a /J·kmol^{-1}	ΔV /m^3·kmol^{-1}
Chain initiation	$R_0 + M \xrightarrow{k_i} R_1$	1.25×10^8	3.38×10^7	−0.020
Chain propagation	$R_n + M \xrightarrow{k_p} R_{n+1}$	1.25×10^8	3.38×10^7	−0.020
Chain transfer to monomer	$R_n + M \xrightarrow{k_{tm}} D_n + R_1$	1.25×10^5	3.38×10^7	−0.020
Chain transfer to polymer	$R_n + D_m \xrightarrow{k_{tp}} D_n + R_m$	4.38×10^8	5.49×10^7	0.0044
Chain transfer to solvent	$R_n + S \xrightarrow{k_{ts}} D_n + R_1$	2.62×10^7	4.97×10^7	−0.020
Chain terminated by disproportionation	$R_n + R_m \xrightarrow{k_{td}} D_n + D_m$	1.25×10^9	4.18×10^6	0.013
Chain terminated by combination	$R_n + R_m \xrightarrow{k_{tc}} D_{n+m}$	1.25×10^9	4.18×10^6	0.013

mixture of ethylene–LDPE respectively, with the unit of kg·m^{-3}. T_0 represents the temperature of feeds in industry, with the unit of K. $C_{p,m}$ represents the average heat capacity, with the unit of kJ·kg^{-1}·K^{-1}. q represents the reaction heat of the polymerization, with the unit of kJ·kg^{-1}. X_E represents the mass fraction of ethylene in the mixture. M_E represents the molar weight of ethylene, with the unit of kg·kmol^{-1}.

$$\rho_E = 6811 - 601.2\ \lg P - 3283\ \lg T + 335.8\ \lg P \cdot \lg T \tag{25}$$

$$\rho_{LDPE} = \frac{1}{9.61 \times 10^{-4} + 7 \times 10^{-7} T - 5.2 \times 10^{-13} P} \tag{26}$$

$$X_E = 1 - \frac{C_{p,m}(T - T_0)}{q} \tag{27}$$

$$\rho_m = \left(\frac{X_E}{\rho_E} + \frac{1 - X_E}{\rho_{LDPE}} \right)^{-1} \tag{28}$$

$$[M] = \frac{\rho_m \cdot X_E}{M_E} \tag{29}$$

Consequently, the ranges of the characteristic time of elementary reactions can be determined, as shown in Table 10. Fig. 15 gives the comparison of the characteristic times of macro-mixing, micro-mixing and elementary reactions, within the industrial operating conditions. It can be found that the delay time t_d is less than $t_{r,i}$, $t_{r,tm}$, $t_{r,tp}$, $t_{r,ts}$ and its range intersects with that of $t_{r,d}$,$t_{r,p}$. The t_M is less than $t_{r,tm}$, but much greater than $t_{r,d}$, and its range intersects with that of $t_{r,i}$, $t_{r,tp}$, $t_{r,ts}$, $t_{r,p}$. Besides, the $\overline{t_m}$ is much less than $t_{r,i}$, $t_{r,p}$, $t_{r,tm}$, $t_{r,tp}$, $t_{r,ts}$, but close to $t_{r,d}$. Thus, the reactions of chain initiation, chain propagation, chain transfer to polymer and chain transfer to solvent are significantly affected by the macro-mixing behavior in the LDPE autoclave reactor, while the reaction of initiator decomposition is affected not only by the macro-mixing behavior, but also by the quality of micro-mixing in the reactor. Consequently, it can be concluded that the product properties of LDPE are dominated by the macro-mixing characteristics of fluid, and the consumption of initiators is affected by both the macro-mixing and micro-mixing characteristics in the LDPE autoclave reactor.

Table 10
The characteristic time of elementary reactions in the LDPE autoclave reactor.

Elementary reactions	Characteristic time t_r/s	
	min	max
Initiator decomposition	9.27×10^{-3}	1.62
Chain initiation	7.45×10^{1}	–
Chain propagation	2.67×10^{-1}	–
Chain transfer to monomer	2.67×10^{2}	–
Chain transfer to polymer	2.86×10^{1}	–
Chain transfer to solvent	4.15×10^{1}	–
Chain terminated by disproportionation	2.18×10^{-4}	–
Chain terminated by combination	2.18×10^{-4}	–

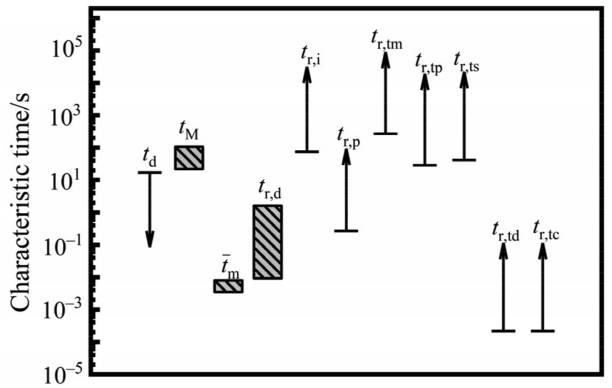

Fig. 15. The characteristic times of macro-mixing, micro-mixing and elementary reactions in the LDPE autoclave reactor.

As it is, the inconsistencies related to effects of macro-mixing and micro-mixing behaviors in the previous works are mainly induced by the fact that different authors focus on different elementary reactions, and the characteristic time of these reactions differ significantly in the order of magnitudes. Besides, according to Fig. 15, the micro-mixing state in the reactor may not affect the weight-averaged molecular weight of LDPE products, and those opposite results in literature may need more evaluation. Perhaps the reactor model, experimental set-ups or conditions investigated in these literatures deviate significantly from industrial reality.

5. Conclusions

This work investigated the macro-mixing and micro-mixing behaviors in an LDPE autoclave reactor by cold-flow experiments and well-verified simulations. Furthermore, the effects of macro-mixing and micro-mixing behaviors on the high-pressure ethylene polymerization were analyzed by comparing the characteristic times of macro-mixing, micro-mixing and elementary reactions. The main conclusions are shown as follows.

(1) Based on the delay time t_d and macro-mixing time t_M calculated from the tracer concentration response curve $c(t) \sim t$, it was observed that the macro-mixing behavior in the reactor was significantly affected by the tracer-injection position and *Re*. The macro-mixing states of feeds inlet0, inlet1 are almost identical, while those of feeds inlet1, inlet2

and inlet3 are quite different. Along with the increase of *Re*, the t_M of feeds inlet0, inlet1 at the positions above the middle bearing increases, while that at the positions below the middle bearing decreases. The t_M of feeds inlet2, inlet3 at both the positions above and below the middle bearing increases as *Re* increases. Besides, for each feed, the t_d at the positions farther away from the feeding point is greater, and the t_d decreases as *Re* increases. Within the range of industrial operating conditions, the t_d ranges from 0 to 17 s, and the t_M ranges from 22 to 107 s.

(2) Based on the segregation index X_s and micro-mixing time t_m, the micro-mixing state at different axial positions in the reactor are similar, but significantly affected by the fluid transport properties (μ, ρ) and agitator rotation speed *N*. Using *Re* to characterize the comprehensive effects of μ, ρ and *N* on the $\overline{X_s}$, $\overline{t_m}$ in the reactor, they both decreased with the increase of *Re*, and the corresponding fitting model were further established. Within the range of industrial operating conditions, the $\overline{t_m}$ ranges from 3.50×10^{-3} to 8.04×10^{-3} s.

(3) Within the range of industrial operating conditions, the characteristic times of various elementary reactions were calculated and compared with that of macro-mixing and micro-mixing (t_d, t_M, $\overline{t_m}$). The comparison revealed that the reactions of chain initiation, chain propagation and chain transfer to polymer are significantly affected by the macro-mixing behavior, while the reaction of initiator decomposition is affected not only by the macro-mixing behavior, but also by the micro-mixing behavior. Thus, the molecular structure of LDPE products is dominated by the macro-mixing, and the consumption of initiators is affected by both the macro-mixing and micro-mixing.

CRediT Authorship Contribution Statement

Zhenchao Tang: Writing – review & editing, Writing – original draft, Visualization, Validation, Resources, Methodology, Investigation, Formal analysis, Data curation. Yuliang Wang: Investigation, Data curation. Zhengliang Huang: Supervision, Project administration. Yao Yang: Supervision, Project administration, Funding acquisition, Conceptualization. Xiaoqiang Fan: Supervision, Resources, Project administration, Methodology, Conceptualization. Binbo Jiang: Supervision, Project administration. Jingdai Wang: Supervision, Project administration. Yongrong Yang: Supervision, Project administration.

Declaration of Competing Interest

The authors declare that they have no known competing financial interests or personal relationships that could have appeared to influence the work reported in this paper.

Acknowledgements

The authors gratefully acknowledge the support and encouragement of the Key Projects of the Ministry of Industry and Information Technology of China (TC220A04W-3, 188).

References

[1] A.J. Peacock, Handbook of Polyethylene: Structures, Properties, and Applications, CRC Press, Boca Raton, 2000.
[2] P. Pladis, C. Kiparissides, A comprehensive model for the calculation of molecular weight–long-chain branching distribution in free-radical polymerizations, *Chem. Eng. Sci.* 53 (18) (1998) 3315–3333.
[3] N. Yaghini, P.D. Iedema, Predicting molecular weight distribution by deterministic modeling and Monte Carlo simulations of radical polymerization with branching and scission allowing for multiradicals and gelation in various reactor configurations, *Chem. Eng. Sci.* 130 (2015) 310–318.
[4] W. Zhou, E. Marshall, L. Oshinowo, Modeling LDPE tubular and autoclave reactors, *Ind. Eng. Chem. Res.* 40 (23) (2001) 5533–5542.
[5] L. Marini, C. Georgakis, Low-density polyethylene vessel reactors: Part I: Steady state and dynamic modelling, *AIChE J.* 30 (3) (1984) 401–408.
[6] S. Ochs, P. Rosendorf, I. Hyanek, X.M. Zhang, W.H. Ray, Dynamic flowsheet modeling of polymerization processes using POLYRED, *Comput. Chem. Eng.* 20 (6–7) (1996) 657–663.
[7] S.X. Zhang, W.H. Ray, Modeling of imperfect mixing and its effects on polymer properties, *AIChE J.* 43 (5) (1997) 1265–1277.
[8] C.M. Villa, J.O. Dihora, W. Harmon Ray, Effects of imperfect mixing on low-density polyethylene reactor dynamics, *AIChE J.* 44 (7) (1998) 1646–1656.
[9] C. Kiparissides, G. Verros, J.F. MacGregor, Mathematical modeling, optimization, and quality control of high-pressure ethylene polymerization reactors, *J. Macromol. Sci.* C33 (4) (1993) 437–527.
[10] X.X. Duan, D. Cheng, J.C. Cheng, X. Feng, C. Yang, Research progress on macro- and micro-mixing and intensification in stirred tank reactors, *Chem. React. Eng. Technol.* 29 (3) (2013) 238–246.
[11] R. Phillips, S. Rohani, J. Baldyga, Micromixing in a single-feed semi-batch precipitation process, *AIChE J.* 45 (1) (1999) 82–92.
[12] L. Smit, The use of micromixing calculations in LDPE-reactor modelling, *DECHEMA Monogr.* 127 (1992) 77–92.
[13] G. Tosun, A mathematical model of mixing and polymerization in a semibatch stirred-tank reactor, *AIChE J.* 38 (3) (1992) 425–437.
[14] R. Pohorecki, J. Baldyga, New model of micromixing in chemical reactors. 2. Application to a stirred tank reactor, *Ind. Eng. Chem. Fundam.* 22 (4) (1983) 398–405.
[15] R. Pohorecki, J. Baldyga, New model of micromixing in chemical reactors. 1. General development and application to a tubular reactor, *Ind. Eng. Chem. Fundam.* 22 (4) (1983) 392–397.
[16] P. Pladis, C. Kiparissides, 110th Anniversary: Nonideal mixing phenomena in high-pressure low-density polyethylene autoclaves: Prediction of variable initiator efficiency and ethylene decomposition, *Ind. Eng. Chem. Res.* 58 (29) (2019) 13093–13111.
[17] A.S. Lobasov, A.V. Minakov, Analyzing mixing quality in a T-shaped micromixer for different fluids properties through numerical simulation, *Chem. Eng. Process. Intensif.* 124 (2018) 11–23.
[18] S. Tomasi Masoni, M. Antognoli, A. Mariotti, R. Mauri, M.V. Salvetti, C. Galletti, E. Brunazzi, Flow regimes, mixing and reaction yield of a mixture in an X-microreactor, *Chem. Eng. J.* 437 (2022) 135113.
[19] Z.M. Chen, P. Zhang, Z.C. Tang, X.Q. Fan, Y. Yang, B.B. Jiang, Z.L. Huang, J.D. Wang, Y.R. Yang, Controlling law of flow and mixing behavior in an autoclave for the production of low-density polyethylene, *Ind. Eng. Chem. Res.* 63 (41) (2024) 17691–17704.
[20] K. Wang, L.F. Feng, Design of Mixing Equipment, China Machine Press, Beijing, 2000.
[21] K. Wang, J. Yu, Stirring Equipment, Chemical Industry Press, Beijing, 2003.
[22] K. Jairamdas, A. Bhalerao, M.B. Machado, S.M. Kresta, Blend time measurement in the confined impeller stirred tank, *Chem. Eng. Technol.* 42 (8) (2019) 1594–1601.
[23] H. Kramers, G.M. Baars, W.H. Knoll, A comparative study on the rate of mixing in stirred tanks, *Chem. Eng. Sci.* 2 (1) (1953) 35–42.
[24] P.V. Danckwerts, Continuous flow systems: Distribution of residence times, *Chem. Eng. Sci.* 2 (1) (1953) 1–13.
[25] M. Antognoli, S. Tomasi Masoni, A. Mariotti, R. Mauri, E. Brunazzi, C. Galletti, Investigation on steady regimes in a X-shaped micromixer fed with water and ethanol, *Chem. Eng. Sci.* 248 (2022) 117254.
[26] H.J. Zheng, Z.L. Huang, Z.W. Liao, J.D. Wang, Y.R. Yang, Y.L. Wang, Computational fluid dynamics simulations and experimental validation of macromixing and flow characteristics in low-density polyethylene autoclave reactors, *Ind. Eng. Chem. Res.* 53 (38) (2014) 14865–14875.
[27] S.F. Reinecke, A. Deutschmann, K. Jobst, U. Hampel, Macro-mixing characterisation of a stirred model fermenter of non-Newtonian liquid by flow following sensor particles and ERT, *Chem. Eng. Res. Des.* 118 (2017) 1–11.
[28] P. Mavros, C. Xuereb, I. Fort, J. Bertrand, Investigation by laser Doppler velocimetry of the effects of liquid flow rates and feed positions on the flow patterns induced in a stirred tank by an axial-flow impeller, *Chem. Eng. Sci.* 57 (18) (2002) 3939–3952.
[29] S. Corrsin, The isotropic turbulent mixer: Part II. Arbitrary Schmidt number, *AIChE J.* 10 (6) (1964) 870–877.
[30] J. Baldyga, J.R. Bourne, Simplification of micromixing calculations. I. Derivation and application of new model, *Chem. Eng. J.* 42 (2) (1989) 83–92.
[31] J.R. Bourne, F. Kozicki, P. Rys, Mixing and fast chemical reaction—I. Test reactions to determine segregation, *Chem. Eng. Sci.* 36 (10) (1981) 1643–1648.
[32] M.C. Fournier, L. Falk, J. Villermaux, A new parallel competing reaction system for assessing micromixing efficiency—Experimental approach, *Chem. Eng. Sci.* 51 (22) (1996) 5053–5064.
[33] B.Q. Liu, M.M. Wang, J.L. Liu, L.Y. Qian, Z.J. Jin, Experimental study on micromixing characteristics of novel large-double-blade impeller, *Chem. Eng. Sci.* 123 (2015) 641–647.

[34] M. Assirelli, W. Bujalski, A. Eaglesham, A.W. Nienow, Study of micromixing in a stirred tank using a Rushton turbine comparison of feed positions and other mixing devices, *Chem. Eng. Res. Des.* 80 (8) (2002) 855–863.
[35] J.M. Rousseaux, L. Falk, H. Muhr, E. Plasari, Micromixing efficiency of a novel sliding-surface mixing device, *AIChE J.* 45 (10) (1999) 2203–2213.
[36] P.V. Danckwerts, The definition and measurement of some characteristics of mixtures, *Appl. Sci. Res. Sect. A* 3 (4) (1952) 279–296.
[37] D.A. Palmer, R.W. Ramette, R.E. Mesmer, Triiodide ion formation equilibrium and activity coefficients in aqueous solution, *J. Solut. Chem.* 13 (9) (1984) 673–683.
[38] P. Costa, C. Trevissoi, Reactions with non-linear kinetics in partially segregated fluids, *Chem. Eng. Sci.* 27 (11) (1972) 2041–2054.
[39] J.M. Ottino, Lamellar mixing models for structured chemical reactions and their relationship to statistical models: Macro- and micromixing and the problem of averages, *Chem. Eng. Sci.* 35 (6) (1980) 1377–1381.
[40] J. Villermaux, Micromixing phenomena in stirred reactors, *Encyclopedia of Fluid Mechanics* 2 (1986) 707–771.
[41] M. Kinzl, G. Luft, R. Horst, B.A. Wolf, Viscosity of solutions of low-density polyethylene in ethylene as a function of temperature and pressure, *J. Rheol.* 47 (4) (2003) 869–877.
[42] M. Coroneo, G. Montante, A. Paglianti, F. Magelli, CFD prediction of fluid flow and mixing in stirred tanks: Numerical issues about the RANS simulations, *Comput. Chem. Eng.* 35 (10) (2011) 1959–1968.
[43] S. Murthy Shekhar, S. Jayanti, CFD study of power and mixing time for paddle mixing in unbaffled vessels, *Chem. Eng. Res. Des.* 80 (5) (2002) 482–498.
[44] J.R. Bourne, Mixing on the molecular scale (micromixing), *Chem. Eng. Sci.* 38 (1) (1983) 5–8.
[45] J. Bourne, P. Dell'Ava, Micro-and macro-mixing in stirred tank reactors of different sizes, *Chem. Eng. Res. Des.* 65 (1987) 180–186.
[46] N.K. Read, S.X. Zhang, W.H. Ray, Simulations of a LDPE reactor using computational fluid dynamics, *AIChE J.* 43 (1) (1997) 104–117.